Miniature all-glass robust pressure sensor

E. Cibula[1], S. Pevec[1], B. Lenardič[2], É. Pinet[3] and D. Đonlagić[1*]

[1]*University of Maribor, Faculty of EE & Computer Science, Smetanova 17, SI-2000 Maribor (Slovenia)*
[2]*Optacore d.o.o., Trpinčeva ul. 39, 1000 Ljubljana (Slovenia)*
[3]*FISO Technologies, 500-195 av. St-Jean-Baptiste, G2E 5R9 Québec (Canada)*
**Corresponding author: ddonlagic@uni-mb.si*

Abstract: This paper describes a newly designed all-glass miniature (Ø 125 µm) fiber-optic pressure sensor design that is appropriate for high-volume manufacturing. The fabrication process is based on the chemical etching of specially-designed silica optical fiber, and involves a low number of critical production operations. The presented sensor design can be used with either single-mode or multi-mode lead-in fiber and is compatible with various types of available signal processing techniques. A practical sensor sensitivity exceeding 1000 nm/bar was achieved experimentally, which makes this sensor suitable for low-pressure measurements. The sensor showed high mechanical stability, good quality of optical surfaces, and very high tolerance to pressure overload.

©2009 Optical Society of America

OSCI codes: (060.2370) Fiber optics sensors; (120.2230) Fabry-Perot

References and links

1. É. Pinet, "Medical applications / Saving lives," Nature Photon., Tech. Focus (special edition on fiber-optic sensors) **2**, 150-152 (2008).
2. J. S. Heo and J. O. Lim, "A micro total reflective extrinsic Fabry-Perot interferometric fiber optic pressure sensor for medical application," Int. J. Mod. Phys. B, **17**, 1199 1204 (2003).
3. O. Tohyama, M. Kohashi, M. Sugihara, and H. Itoh, "A fiber-optic pressure microsensor for biomedical applications," Sens. Actuators A, **66**, 150-154 (1998).
4. T. Bae, R. A. Atkins, H. F. Taylor, and W. N. Gibler, "Interferometric fiber-optic sensor embedded in spark plug for in-cylinder pressure measurement in engines," Appl. Opt. **42**, 1003 1007 (2003).
5. S.H. Aref, H.Latifi, M.I. Zibaii, and M. Afshari, "Fiber optic Fabry-Perot pressure sensor with low sensitivity to temperature changes for downhole application," Opt. Commun. **269**, 322 330 (2007).
6. B. Glišić and D. Inaudi, in *Fibre optic methods for structural health monitoring*, (J. Wiley & sons Eds., 2007).
7. www.fiso.com,
8. K. Totsu, Y. Haga, and M. Esashi, "Ultra-miniature fiber-optic pressure sensor using white light interferometry," J. Micromech. Microeng. **15**, 71-75 (2005).
9. D. C. Abeysinghe, S. Dasgupta, J. T. Boyd, and H. E. Jackson, "A novel MEMS pressure sensor fabricated on an optical fiber," IEEE Photon. Technol. Lett. **13**, 993-995 (2001).
10. E. Cibula and D. Đonlagić, "Miniature fiber-optic pressure sensor with a polymer diaphragm," Appl. Opt. **44**, 2736-2744 (2005)
11. D. Đonlagić and E. Cibula, "All-fiber high-sensitivity pressure sensor with SiO_2 diaphragm," Opt. Lett. **30**, 2071-2073 (2005).
12. X. Wang, J. Xu, Y. Zhu, L. K. Cooper, and A. Wang, "All-fused-silica miniature optical fiber tip pressure sensor," Opt. Lett. **31**, 885-887 (2006).
13. Y. Zhu, K. L. Cooper, G. R. Pickrell, and A. Wang, "High-temperature fiber-tip pressure sensor," IEEE J. Lightwave Technol. **24**, 861-869 (2006).
14. J. Xu, X. Wang, K. L. Cooper, G. R. Pickrell, and A. Wang, "Miniature temperature-insensitive Fabry-Pérot fiber-optic pressure sensor," IEEE Photon. Technol. Lett. **18**, 1134-1136 (2006).
15. C. Belleville and G. Duplain, "Fabry-Perot optical sensing device for measuring a physical parameter," US Patents #5,202,939 (1993) and #5,392,117 (1995).
16. M. Di Giovanni, in *Flat and corrugated diaphragm design handbook* (L.L. Faulkner and S.B. Menkes Eds., CRC Press, 1982), Chap. 12 "Bending of diaphragms under lateral pressure," 130-156.

1 Introduction

Optical fiber pressure sensors possess distinct advantages over their electrical counterparts such as small dimensions, cylindrical geometry, electromagnetic immunity, all-dielectric

#106994 - $15.00 USD Received 30 Jan 2009; revised 4 Mar 2009; accepted 5 Mar 2009; published 16 Mar 2009

design, possibility to operate at elevated temperatures and compatibility with various types of harsh environments. This makes fiber pressure sensors very attractive for a variety of applications from biomedical field [1-3] to the automotive industry [4] or civil engineering [5, 6]. Therefore, significant efforts have been devoted to the development and evolution of these types of sensors into practical products.

The commercial solutions currently available mostly rely on adding external components to the optical fiber's end. For example, micro-machined opto-mechanical systems (MOMS) diced into small silicon-based chips mounted at the tips of optical fibers are successfully used for the mass-production of miniature fiber-optic pressure sensors [7]. The drawback of this approach is the sensor's diameter, which is larger than a standard fiber diameter, although some silicon-based ultra-miniature pressure sensors have been reported [8]. Additionally, the applications of bonding materials such as polymeric adhesives, necessary for attaching the pressure silicon-based chip to the optical fiber tip, limit the temperature range and long-term stability of these sensors.

Recently, significant efforts have been devoted to reducing the size of the fiber pressure sensor down to the optical fiber diameter range. One of the earliest works proposed relied on the creation of an optical cavity performed by photolithographic process at the end-face of a 400 μm diameter optical fiber, and on the anodic bonding of a silicon diaphragm to create a Fabry-Pérot (F-P) resonator [9]. Although very innovative and suitable for laboratory research work, such technology could not easily be transferred to industrial mass-production processes due to technical and practical limitations.

The successful reduction of sensor diameter down to the Ø 125 μm range using simple manufacturing steps was achieved with selective chemical etching of doped silica core to create a cavity at the tip of an optical fiber [10]. In this study, a flexible polymer diaphragm was then laid over the tip cavity by a "dip and evaporate" technique to finally form a F-P cavity. This work was later extended to all-SiO_2 sensor designs, where the polymer diaphragm was replaced by the silica diaphragm [11]. Similar techniques for the production of all-SiO_2 pressure sensors based on the splicing of fiber size capillaries were also proposed by other groups [12-14].

All recently reported techniques that allow the manufacturing of true all-fiber miniature SiO_2 diaphragm sensors unfortunately involve a substantial number of fusion splices, precision cleaves, and micrometer length adjustments of spliced fiber segments [10-14]. With a large number of manufacturing steps that are not so easy to automate and additionally that have limited production yields, the proposed miniature sensor designs remained mainly inappropriate for realistic and economic industrial manufacturing.

In this paper, we present a new all-glass miniature fiber optic sensor design that is based on a specially developed sensor-forming fiber. The introduction of sensor-forming fiber allows for a significant reduction of critical and time-consuming production steps, particularly eliminating the need for precision length adjustment of critical sensor constituents. The necessary sensor's constituent length adjustments are replaced by time-controlled chemical etching that can be done in large batches. The proposed approach also increases the assembly yield and makes the production process appropriate for practical mass-production manufacturing, while simultaneously allowing for the design of high sensitivity pressure sensors.

2 Sensors production process description

The practical assembly of the sensor is achieved over only three steps, which are summarized in Fig. 1.

#106994 - $15.00 USD Received 30 Jan 2009; revised 4 Mar 2009; accepted 5 Mar 2009; published 16 Mar 2009
(C) 2009 OSA

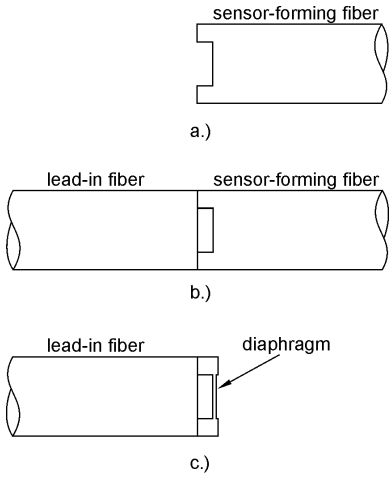

Fig. 1. The pressure sensor simplified fabrication process is performed over only 3 steps: (a) formation of the cavity, (b) fusion splicing with the lead-in fiber and (c) creation of the diaphragm

In the first step, a cavity is micro-machined at the tip of a cleaved optical fiber with well-defined depth and diameter. The cavity is created by the selective chemical etching of a custom-designed sensor-forming optical fiber. This sensor-forming fiber has a germanium-doped step index core with a diameter of 90 μm and a refractive index difference of about 0.7% (corresponding to 7.42% mol of GeO_2). When this fiber is exposed to 40% HF at 25°C, the doped region etches at a rate of about 2.8 μm/min, while the pure silica cladding etches at a rate of about 1 μm/min. The higher etching rate of the doped core region results in a cavity formation at the tip of the fiber, as shown in Fig.1(a). The cavity depth is simply controlled by etching time. Depending on the desired cavity depth, the sensor-forming fiber is drawn to a larger initial diameter in such a way as to achieve a standard 125 μm fiber outer diameter after completion of the chemical etching phase. For example, when a target cavity depth of 12 μm was selected, the starting (initial) sensor-fiber diameter corresponded to 138 μm and the etching took 6.5 min in 40% HF at 25°C. Various cavity depths were produced by using different etching times and different initial outer diameters of the sensor-forming fiber.

This first step can be carried-out in larger production batches while providing highly consistent cavity depths created at the tips of the optical fibers. This eliminates any need for individual cavity length adjustments or inspection. An additional advantage of this chemical etching process compared to depth control achieved by mechanical polishing relates to the fact that the formed cavity is always clean and free from polishing debris, which further simplifies the manufacturing process and avoids complex and hard to control cleaning steps.

The sensor-forming fiber was produced by the modified chemical vapor deposition (MCVD) process, with an increased number of deposition layers compared to the fabrication of a similar-sized standard multi-mode preform. The large number of thin deposition layers and the low germanium concentration allowed for low fiber profile ripple, which resulted in low surface roughness after etching, as shown in Fig. 2(a). The surface roughness is caused by slight variations in composition within individual core deposition layers, resulting in an uneven etching rate over the core region.

In the second step, the etched sensor-forming fiber is fusion-spliced to the lead-in fiber, as shown in Fig. 1(b). Any desired type of lead-in fiber can be used depending on the signal-processing technique. In our investigation, both standard single-mode and standard 50 μm multi-mode fibers were used. The latter ones are of particular interest since they provide full compatibility of the sensor with commercially-available signal processors based on white-light interferometry [15], and supplied by *FISO Technologies Inc.* [7]. Fusion splicing of the sensor with a large air cavity required the development of appropriate splicing recipes, in

#106994 - $15.00 USD Received 30 Jan 2009; revised 4 Mar 2009; accepted 5 Mar 2009; published 16 Mar 2009
(C) 2009 OSA

order to achieve good fusion between the two fibers whilst maintaining the structural and mechanical integrity of the entrapped air cavity. The production process results in fully sealed cavity and the sensor can be used for static pressure measurements.

Fusion splicing is also used to fire-polish the inner surface of the cavity that becomes rough after chemical etching due to ring MCVD layers, as previously explained. If fire-polishing is not done, the surface roughness significantly reduces the reflectivity of the cavity's surface. Fire polishing is achieved by heating the spliced region for several seconds after completion of the prime splicing procedure. Since germanium-doped regions possess lower viscosity than pure silica, the cavity end surface can be smoothed out by surface tension, while the cavity walls composed of pure silica maintain sensor structural integrity during fire-polishing step. The cavity end-surface qualities before and after fire-polishing based on optimized fusion splicing procedure, are shown in Fig. 2.

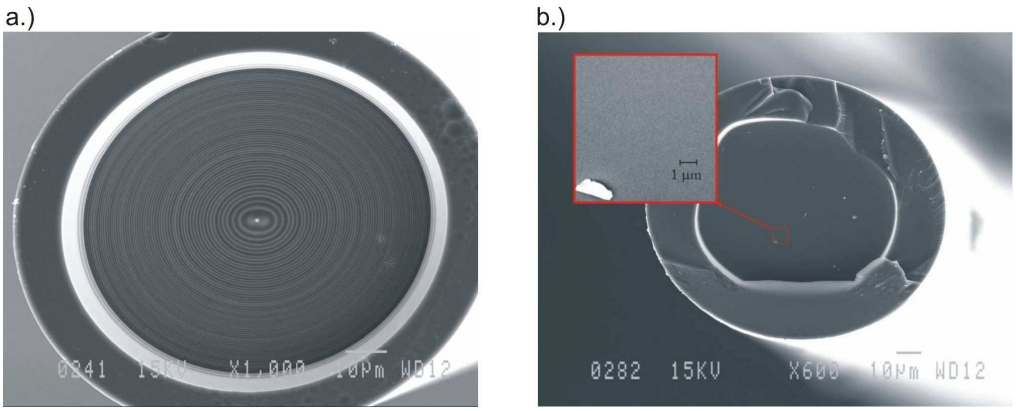

Fig. 2. SEM photos of the etched cavity: (a) before fire-polishing and (b) after fi re-polishing

Fire-polishing using fusion splicing however proved to be an unstable and poorly repeatable process. The same set of fusion parameters resulted in very different fringe visibilities even when identical fibers were consecutively spliced. This is shown in Fig. 3 where three sensor-forming fibers etched within the same batch were spliced to the same type of lead-in fiber.

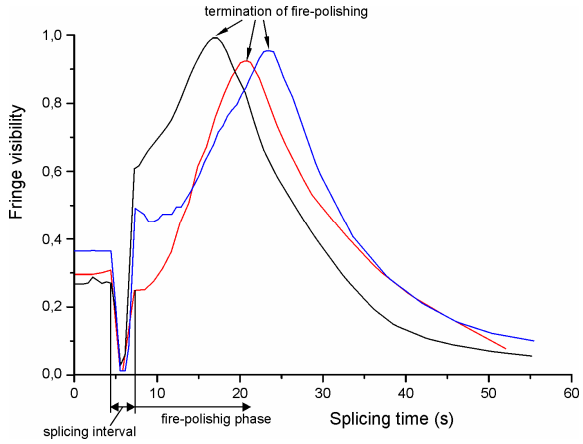

Fig. 3. Changes of sensor fringe visibility during splicing and fire-polishing for 3 different sensor-forming fibers obtained from the same batch

#106994 - $15.00 USD Received 30 Jan 2009; revised 4 Mar 2009; accepted 5 Mar 2009; published 16 Mar 2009
(C) 2009 OSA

Figure 3 shows fringe visibility of the spliced cavity versus splicing time (the fringe visibility was on-line measured using an optical spectrum analyzer under low-coherence illumination). The splicing was performed on *Ericsson* FSU 925 fusion splicer with typical fusion parameters (*fusion time/current*), as follows: 0.2 s/13 mA, 0.8 s/9.5 mA, 60 s/7.2 mA, and with a closing gap of 50 μm and an overlap of 5 μm. The first and second high-current intervals represent the splicing phase, while the third low-current, long-duration interval corresponds to the fire-polishing sequence.

Figure 3 indicates the rapid rise and drop in fringe visibility during the fire-polishing sequence. The well-pronounced maximum occurs randomly over time and could originate from the potential instability of the plasma occurring between the arc-splicing electrodes. In order to obtain a consistent and high yield splicing procedure, a feedback loop was therefore introduced into the splicing process, as shown in Fig. 4.

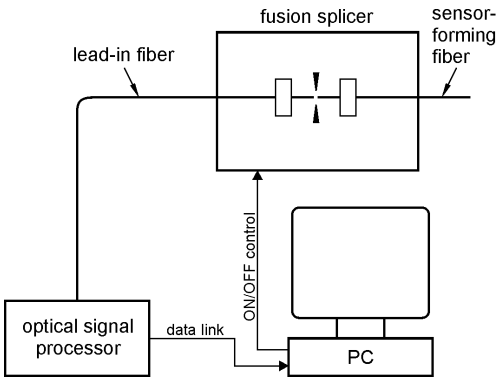

Fig. 4. Computer-controlled splicing setup

The on-line measuring of fringe visibility was performed during splicing and a computer algorithm was used to detect the peak of the fringe contrast in order to automatically terminate the splicing process (we slightly modified FSU 925 for this purpose to allow external computer controlled termination of the fusion process).

Repeatable reflectivities of the F-P surfaces not far from the theoretical limit were obtained by applying of a feedback-assisted fire-polishing step. Fringe visibility of over 90% was achieved for over 90% of all produced samples.

In the third fabrication step, the sensor-forming fiber is cleaved near the fusion splice with the help of visual inspection under a microscope, and is polished to form a pressure-sensitive diaphragm (Fig. 1(c)). Fiber cleaving is typically performed about 20 μm away from the splice. This value is the minimum distance that provides repeatable cleaves with common scratch-and-cleave procedure, mainly due to the uneven stress distribution in the sensor-fiber caused by the presence of the air cavity. This precision cleaving procedure is already described in detail [10]. While we performed the cleaving step manually, the cavity is easy to locate under optical microscope, as shown in Fig. 5, and thus allows for straightforward automation of cleaving process by application of modern machine vision tools. Controlled-polishing is performed in an enclosed chamber where the pressure is cyclically varied, while the response of the sensor is observed by a signal processor. Using this approach, diaphragm deflections of up to 50 nm/bar were typically achieved, which represent sufficient sensitivity for a variety of practical industrial applications. By using our custom build polishing setup, we were able to complete polishing step in less than 3 minutes. Further automation and development of polishing tools could likely make this time even shorter.

#106994 - $15.00 USD Received 30 Jan 2009; revised 4 Mar 2009; accepted 5 Mar 2009; published 16 Mar 2009
(C) 2009 OSA

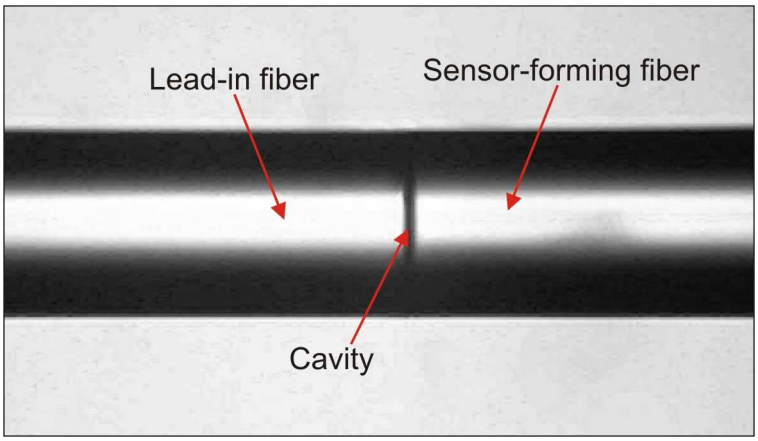

Fig. 5. Cavity formed by fusion splicing of etched fiber is easy to identify by optical microscope

Higher sensitivity can be achieved by an additional fabrication step where etching in HF is used to fine-tune the diaphragm thickness. This step was performed in a closed vessel with controlled pressure. The sensor response is observed during etching in 10% HF acid while the pressure is cyclically varied until the desired sensitivity is achieved, as already described [11].

Figure 6 shows a picture of the produced sensor with a typical 550 nm/bar sensitivity, obtained using a scanning electronic microscope (SEM).

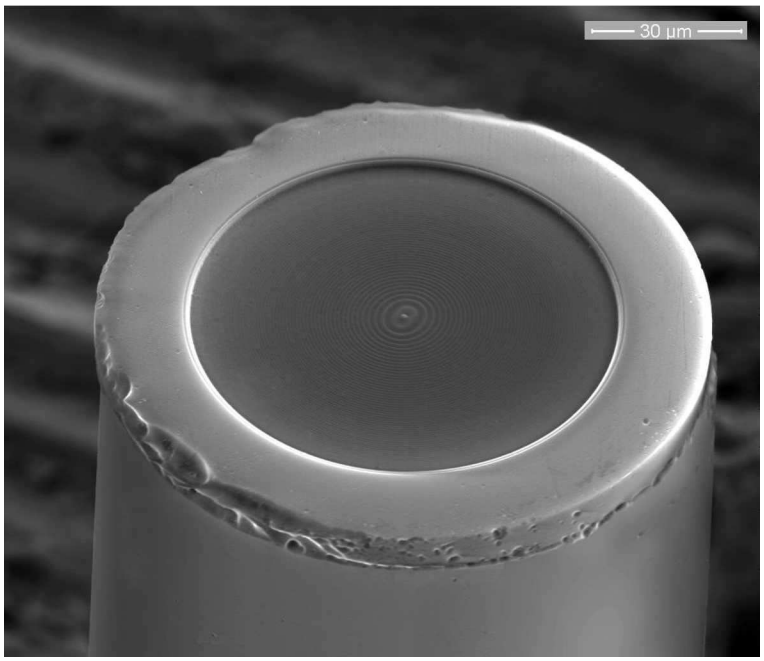

Fig. 6. SEM photo of a typical sensor with a sensitivity of ~550 nm/bar (×2 000)

The diaphragm is retracted within the structure due to the etching of the sensor during the final production phase (since germanium-doped silica diaphragm etching rate is higher than the one of pure silica walls). This feature provides increased mechanical protection of the thin and potentially-sensitive diaphragm, as the edges of the diaphragm are recessed and thus not directly exposed to mechanical shocks that could be encountered during experimental sensor

#106994 - $15.00 USD Received 30 Jan 2009; revised 4 Mar 2009; accepted 5 Mar 2009; published 16 Mar 2009
(C) 2009 OSA

manipulations since more likely the edges and not the more fragile diaphragm will become in contact on a flat surface.

Figure 7 shows a cross-section of the same sensor under SEM, obtained after side-cutting performed by a scanning ion-beam.

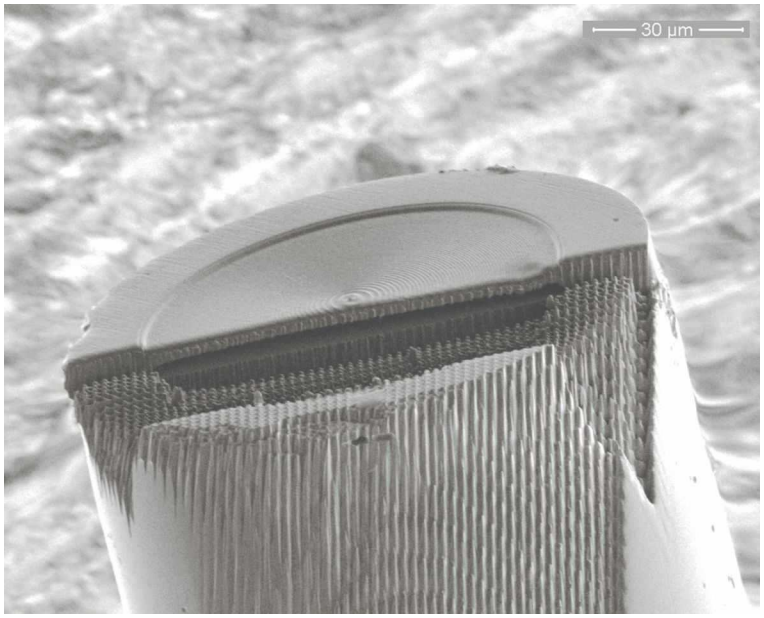

Fig. 7. SEM photo (×2000) of the diaphragm cross-section showing the entrapped air cavity and the suspended recessed diaphragm. The sensor was cut by scanning ion-beam creating the apparent roughness visible in the front of the sensor fiber

This Figure shows a flat and reasonably-uniform recessed silica diaphragm with a thickness of about 2 µm confirming that the proposed sensor design allows the creation of a geometrically well-defined, uniform and very thin silica diaphragm.

3 Experimental section

Since the core of the sensor-forming fiber (*i.e*. corresponding to the final diaphragm) was relatively large, we were able to achieve relatively high sensor sensitivity that exceeded 1000 nm/bar. This sensitivity is about 3 times higher than previously-reported designs for similar types of sensors [11]. Consistent high-production yield (>85%) experimental production was achieved for somewhat lower sensitivities that ranged around 600 nm/bar. Most resolution requirements for biomedical pressure measurements could be met when combining these sensors with commercially-available signal processors like the ones available from *FISO Technologies*.

Figure 8 shows measured diaphragm deflection versus applied pressure for typically-produced sensors with sensitivity of 550 and 1100 nm/bar.

The sensor with lower sensitivity demonstrates linear characteristics over the biomedical pressure range (up to 0.4 bar), while the high-sensitivity sensor exhibits somewhat non-linear static characteristics. The non-linear behavior is expected however when the diaphragm becomes very thin, especially when its deflection is 5 times greater than its thickness [16].

#106994 - $15.00 USD Received 30 Jan 2009; revised 4 Mar 2009; accepted 5 Mar 2009; published 16 Mar 2009
(C) 2009 OSA

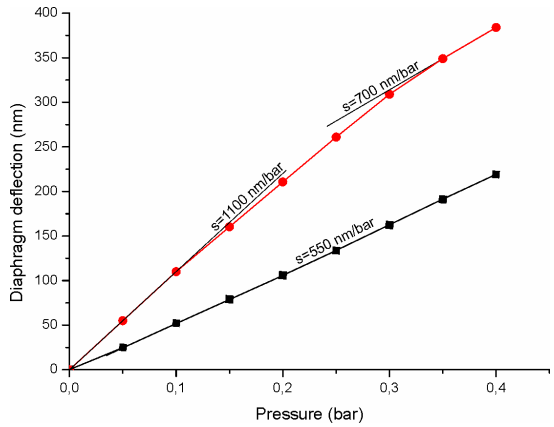

Fig. 8. Deflection of the sensor diaphragm *vs*. pressure for two sensors with different sensitivities

Four sensor samples were used to evaluate their resistance to pressure overload. They were gradually pressurized in hydraulic oil to high pressures until diaphragm cracking occurred (two sensors had a pressure sensitivity of 550 nm/bar and two had a sensitivity of 1100 nm/bar). The pressure was increased gradually in cycles and during each pressurization-depressurization cycle, pressure was increased by 2 bar. The first lower sensitivity sensor was destroyed at 78 bar and the second survived a pressure of 100 bar, which was also the limit for our experimental set-up. Both high-sensitivity sensors survived up to 80 bar. The response characteristic at such high pressures becomes highly non-linear, as shown in Fig. 9.

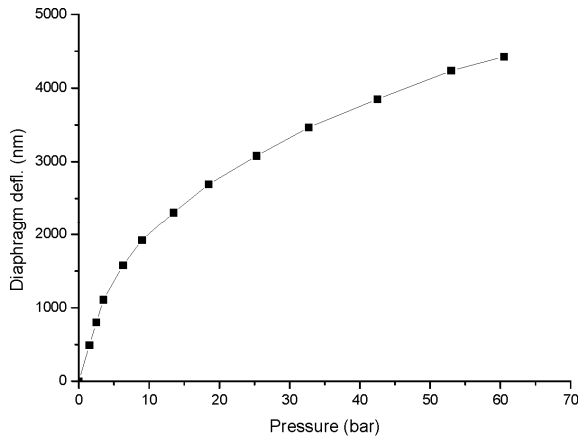

Fig. 9. Deflection of sensor diaphragm *vs*. pressure at high pressures showing non linear behavior (sensor sensitivity 550 nm/bar)

The 1100 nm/bar sensitivity sensors started to show zero-point shift (*e.g*. differences in cavity length before and after pressurization) of 5 nm and 9 nm when the pressurization-depressurization cycle exceeded 70 bar, while the lower sensitivity sensors showed a zero-point shift that remained less than 2 nm up to their destruction. This is a considerably different behavior than the one encountered in conventional metal diaphragm pressure sensors that are known to be highly sensitive to overloads. The durability and resistance of the proposed sensors to the overloads can be attributed to the high elasticity of silica, and a smooth, fire-polished, micro-crack-free inner diaphragm surface.

Additionally, the measured sensor temperature dependence (zero thermal shift) is approximately linear with temperature and is in the range between 0.3 and 0.4 nm/°C. Test in

#106994 - $15.00 USD Received 30 Jan 2009; revised 4 Mar 2009; accepted 5 Mar 2009; published 16 Mar 2009
(C) 2009 OSA

air at atmospheric pressure performed at 200°C during more than 12 h showed a drift of less 1 nm indicating good sensor stability.

4 Summary

This paper presented a design of a fiber-optic pressure sensor that could be produced in few steps. The proposed fabrication process is composed of linear sequence of operations that requires only one splicing, one cleaving step and a final treatment of the membrane to achieve high sensitivity. All steps can be highly automated with possibly high-yield production process. While the raw material costs are marginal (only few centimeters of specialty sensor-forming fiber are necessary) the presented approach thus offers a potentially cost-effective design for miniature (Ø 125 µm) all-glass fiber-optic pressure sensors. Selective chemical etching based on a custom-designed sensor-forming fiber allows for a batch-compatible production process that replaces the need for multiple precise length adjustments and multiple fusion steps, as compared to previously-proposed sensors of similar design. The proposed design, therefore, opens realistic possibilities for industrial production and commercialization of all-glass miniature fiber-optic pressure sensors. A sensitivity of 1100 nm/bar was also achieved which is, to our knowledge, the highest all-glass miniature sensor sensitivity reported in the literature. This robust sensor also demonstrated very high resistance to overload, which is an important advantage for practical usage of the sensor in realistic applications. The proposed miniature all-glass pressure sensor design is, therefore, a good candidate for applications where size, cost, material inertness, mechanical and chemical resistance as well as insensitivity to electromagnetic interferences are important concerns.

#106994 - $15.00 USD Received 30 Jan 2009; revised 4 Mar 2009; accepted 5 Mar 2009; published 16 Mar 2009
(C) 2009 OSA